Journal of Power Sources 196 (2011) 8140–8146

Contents lists available at ScienceDirect

Journal of Power Sources

journal homepage: www.elsevier.com/locate/jpowsour

Investigation of the thermal properties of a Li-ion pouch-cell by electrothermal impedance spectroscopy

Jan Philipp Schmidt*, Daniel Manka, Dino Klotz, Ellen Ivers-Tiffée

Institut für Werkstoffe der Elektrotechnik (IWE), Karlsruher Institut für Technologie, Adenauerring 20b, 76131 Karlsruhe, Germany

ARTICLE INFO

Article history:
Received 2 April 2011
Accepted 17 May 2011
Available online 27 May 2011

Keywords:
Electrothermal impedance spectroscopy
Thermal model
Thermal impedance
Li-ion battery

ABSTRACT

Electrothermal impedance spectroscopy (ETIS), is introduced as a new measurement method and thermal parameters derived from a pouch-type lithium-ion cell are presented. ETIS is a valuable tool for (i) the determination of the thermal impedance and (ii) the validation of thermal models. The excitation signal applied to the cell during measurement does not cause a change in entropy, thus facilitating the parameter identification of a thermal model for heat conduction and thermal capacity.

ETIS can be applied to measurements in time domain and in frequency domain. Both approaches are presented and a combination further improves measurement time and accuracy.

1. Introduction

1.1. Motivation

The specifications for lithium-ion batteries depend on the field of application. While for consumer electronics a high energy density with only modest power output is suitable, the drive train of an electric vehicle (EV) is much more demanding in terms of power capabilities. A high generation of heat necessitates cooling concepts to prevent thermal runaway [1–3] and aging processes [4,5].

Heat control of lithium-ion batteries and temperature monitoring of individual cells will ensure performance and safety. Large-format and high-power cells, as required for automotive applications, develop non-uniform temperature distributions during charging and discharging cycles. Surface temperature differs strongly from core temperature. Hence thermal models are of critical importance, which should predict precisely the inside temperature distribution from a measured surface temperature.

The validation of thermal models and the identification of the passive thermal behavior (heat conduction and thermal capacity) is a complex process. For this purpose, we propose the electrothermal impedance spectroscopy (ETIS), which allows to

(a) validate thermal models without the need of a coupled electrochemical model,
(b) determine locally resolved transfer functions (thermal impedance) for variable positions at the cell surface.

Moreover, the thermal properties of a cell with arbitrary geometry and size can be modeled. The proposed ETIS is a nondestructive method, as cell opening for core temperature measurements is not required. In analogy to well-established electrical equivalent circuit models, thermal equivalent circuit models can be easily deduced and parameterized.

1.2. Literature survey

The performance of lithium-ion cells is highly temperature dependent, and performance prediction requires electrochemical models coupled with thermal models. For this purpose mainly finite element models (FEM) are applied [6,7], which comprise the cell design and the cell material properties. The FEM model calculates a spatially, highly resolved temperature distribution by using analytical expressions for heat transfer and generation. All FEM models require high computing capacities, which limit their applicability in thermal management systems for EV.

Computing time can be significantly shortened by using an equivalent circuit model [8,9]. With the electrothermal analogy [10] the thermal capacity can be translated into a capacitance and heat resistance into a resistance. Every thermal system can be described by a thermal impedance that consists of combinations of these elements. If the temperature difference over a thermal system is known the heat flow can be calculated using the thermal impedance and vice versa. Electrical equivalent circuits are already widely spread for electrochemical models and can be eas-

* Corresponding author. Tel.: +49 721 60847583; fax: +49 721 60847492.
E-mail address: jan.schmidt@kit.edu (J.P. Schmidt).

0378-7753/$ – see front matter © 2011 Elsevier B.V. All rights reserved.
doi:10.1016/j.jpowsour.2011.05.047

ily transferred to thermal models. Since molecular diffusion and thermal conduction obey the same mathematical differential equation, equivalent circuit elements describing diffusion can be used for both models. However, the gain in performance is traded for a decrease of the spatial resolution of the temperature distribution.

For both models – FEM and equivalent circuit models – the parameterization and validation is only successful if the electrochemical model for the description of the heat generation is known. However, it is possible to identify the parameters of the thermal model together with an electrochemical model, as reported in [11]. But such an approach increases the number of free parameters significantly. This leads to parameters that are not interpretable by the laws of physics and is associated with a highly instable fit procedure.

A parameterization of the thermal model from charging and discharging cycles is only possible, when the amount of heat generated by polarization and ohmic losses and the change in entropy is known. Otherwise, these values have to be estimated during the parameterization process and as part of an electrochemical model.

The method of electrothermal impedance spectroscopy (ETIS), which is presented here, ties in with the preceding works of Barsoukov et al. [12] and Forgez et al. [9] and extends those. As a result, the corresponding thermal impedance spectrum can be calculated without any a priori assumptions on model order or structure.

2. Time-domain method

A sinusoidal current without an offset will stimulate heat generation, instead of symmetrical current impulses, as done in [9]. The suitable frequency is chosen from the electrochemical impedance spectrum of the cell (cylindrical, pouch or prismatic) with following criteria:

(a) The stimulating frequency has to be two decades higher than the characteristic frequency of the charge transfer process. This boundary condition guarantees no change in entropy and avoids a change of the state of charge (SOC). As a precondition, the frequency range of charge transfer at anode and cathode has to be known [13].
(b) The chosen frequency should only stimulate processes given by ohmic loss contributions (electrolyte, electrodes and current collectors).
(c) The measurement setup has to meet the technical requirements. Usually, for electrochemical impedance spectroscopy low amplitudes are chosen to guarantee linearity and time invariance of the system. However, for ETIS, amplitudes have to be much higher since a temperature increase of the cell is stimulated. Hence, a galvanostat with a sufficient high maximal current and sufficient large frequency bandwidth has to be chosen.

Fig. 1 shows a typical electrochemical impedance spectrum (Nyquist plot) of the commercial cell used. The intersection of the impedance spectrum with the real axis (Re(Z)) at 17 kHz is considered as the sum of ohmic loss contributions.

The heat flow stimulated by the sinusoidal current with constant amplitude I_A in the interior of the cell is calculated from the real part of the impedance Z at the excitation frequency f_i:

$$q = P_{el} = \mathrm{Re}(Z(f_i)) \cdot \left(\frac{I_A}{\sqrt{2}}\right)^2 \quad (1)$$

For simplification the real part of the impedance Z at the excitation frequency f_i will be denoted as R_0 in the following.

Since the impedance is temperature dependent, R_0 will decrease with ongoing excitation due to an increase of the cell temperature

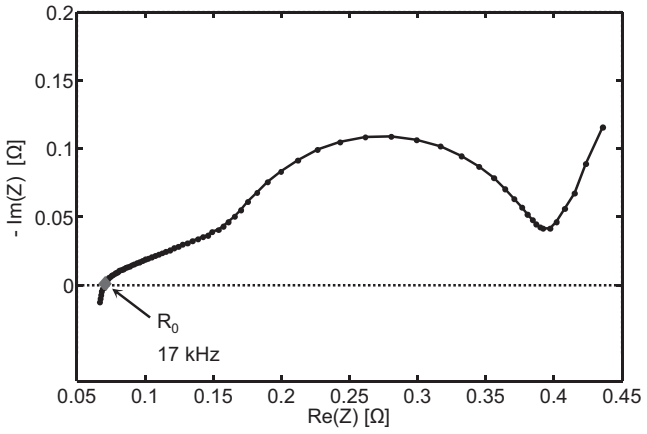

Fig. 1. Electrochemical impedance spectrum of the commercial lithium-ion cell at $T = 23\,^{\circ}\mathrm{C}$, SOC = 5%. The sum of ohmic loss contributions can be read at the intersection of the impedance spectrum with the real axis (Re(Z)) at 17 kHz.

(compare Fig. 2). Therefore the impedance has to be considered time dependent and Eq. (1) is extended as follows.

$$q(t) = R_0(t) \cdot \left(\frac{I_A}{\sqrt{2}}\right)^2 \quad (2)$$

Fig. 2 shows, that for switching on a sinusoidal current with constant amplitude the heat flow does not follow an ideal step function. A step function of the heat flow is only achieved, if the current amplitude is controlled to compensate for the decrease in the impedance. However, and in contrast to [12], the method applied in this work is not restricted to step functions of the heat flow as perturbation signal.

After heat flow is stimulated and the temperature change is measured at an arbitrary position on the cell surface, the heat flow $q(t)$ and a temperature $T_{surf}(t)$ are obtained as functions of time. However the thermal impedance is represented in the frequency domain. Thus a transformation of the time-domain data to frequency domain has to be performed. In system theory, a Laplace transform of the input and output signals is commonly applied to calculate the transfer function as

$$Z(s) = \frac{Y(s)}{X(s)} = \frac{L(y(t))}{L(x(t))} \quad (3)$$

In this equation $x(t)$ and $y(t)$ are the signals in time domain and $X(s)$ and $Y(s)$ are the corresponding Laplace transforms, with s as the Laplace variable:

$$s = j2\pi f \quad (4)$$

To get the transfer function for the thermal system, the heat flow $q(t)$ is chosen as input signal and the temperature on the surface $T_{surf}(t)$ is chosen as output signal.

$$Z_{th}(s) = \frac{T_{surf}(s)}{Q(s)} = \frac{L(T_{surf}(t))}{L(q(t))} \quad (5)$$

After substitution of s with equation (4) the thermal impedance Z_{th} can be approximated by an equivalent circuit model, and elements like resistance and capacitance can be interpreted in terms of a thermal model [10]. By variation of the position of the temperature measurement, different thermal impedance spectra can be obtained, resulting in a spatially resolved thermal impedance.

After substitution of the Laplace variable by Eq. (4), the fast Fourier transformation (FFT) can be applied. This is advantageous, because the FFT is an efficient algorithm available in most numerical computing environments. To solve the problems of spectral leakage and aliasing the thermal impedance is calculated by an

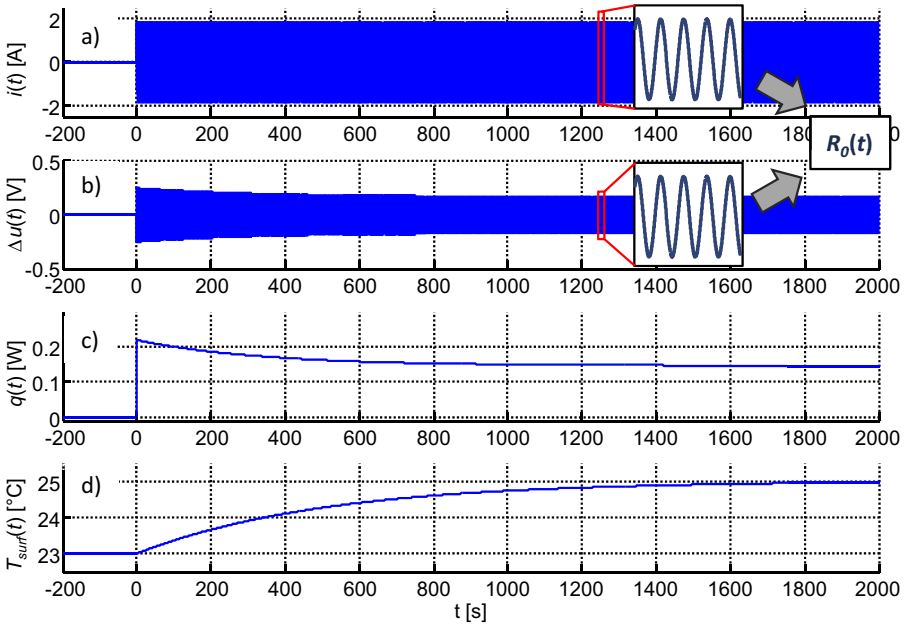

Fig. 2. Simulation of the change in temperature and heat flow when a lithium-ion cell is excited by switching on a sinusoidal current with constant amplitude. (a) Current $i(t)$ as function of time, in magnification the sine function is visible. (b) The overpotential $u(t)$ of the cell as function of time, in magnification the sine function is visible and together with the current the ohmic resistance can be calculated. (c) Heat flow $q(t)$ as function of time. (d) surface temperature of the cell $T_{surf}(t)$ as function of time.

algorithm developed in our group [14], which is based on [15]. In contrast to the approach described in [12] we do not assume a model. This offers two advantages: no restrictions have to be considered regarding the structure or the order of the physical process.

3. Frequency-domain method

The mathematical transformation can be avoided by the generation of a sinusoidal heat flow. Analogous to electrochemical impedance spectroscopy, the thermal impedance is then obtained directly from measured amplitudes and phase angles for different frequencies.

For the well-established electrochemical impedance spectroscopy (EIS) a sinusoidal excitation signal, current or potential, is used. In EIS each single frequency is measured sequentially. As the amplitude of the input signal X_A and the output signal Y_A and the phase shift of the input signal φ_X and output signal φ_Y are known for each frequency, the impedance can be easily calculated using

$$Z_{th}(f_q) = \frac{Y_A(f_q)}{X_A(f_q)} e^{j(\varphi_X(f_q)-\varphi_Y(f_q))} \tag{6}$$

If the input $x_A(t)$ is chosen as the heat flow $q(t)$ and the output $y_A(t)$ is chosen as the surface temperature $T_{surf}(t)$, Eq. (6) can be applied correspondingly to electrothermal impedance spectroscopy. Following Eq. (1) the generated heat is equal to the electrical power dissipation. Since the electrical power dissipation cannot be negative, a constant heat flow q_{const} has to be added to the sine function with the amplitude q_A

$$q(t) = P_{el}(t) = q_A \sin(2\pi f_q t) + q_{const} \tag{7}$$

with

$$q_{const} \geq q_A \tag{8}$$

in order to satisfy the condition

$$P_{el}(t) \geq 0 \tag{9}$$

This is plausible, since for positive and negative sign of the current an ohmic resistor will always generate heat.

From Eqs. (2) and (7), the modulation for the current amplitude can be calculated:

$$I_A(t) = \sqrt{\frac{2}{R_0(t)}(q_A \sin(2\pi f_q t) + q_{const})} \tag{10}$$

The amplitude-modulated excitation current $i(t)$ is depicted schematically in Fig. 3, together with the resulting heat flow $q(t)$ and temperature $T_{surf}(t)$ on the cell surface.

The transient period T_Z is inserted before the actual frequency-domain measurement. During that phase a sinusoidal current with constant amplitude is applied (as during the time-domain measurement). At the end of this phase, the surface temperature of the cell has reached a steady state. Now the amplitude of the current is modulated following Eq. (10). As in electrochemical impedance spectroscopy, a certain number of periods are excluded from the integration, allowing the system to reach a harmonic oscillation. The duration of this phase is denoted as T_E. The subsequent periods T_K are used for evaluation either with Fourier transformation or orthogonal correlation [16]. Accuracy can be improved by increasing the number of measurement periods T_K.

Now, the complete spectrum has to be recorded by repeated amplitude-modulation of the current with different frequencies f_q. The frequency range is limited at high frequencies by the sample rate f_s of the temperature signal.

4. Experimental

The same experimental setup was used for the excitation of the lithium-ion cell with (i) time-domain method and (ii) the frequency-domain method. The pouch cell, a commercial cell with a nominal capacity of 340 mAh, was contacted with a clamping fixture on the tabs, which are made of copper (Cu). The thermal capacities of the tabs are sufficiently large to assure constant temperature conditions during experiments.

The cell was placed in a climate chamber (WK3-340/70, Weiss, Germany) which adjusted ambient and cell temperature at the beginning of the experiment. The climate chamber was turned off

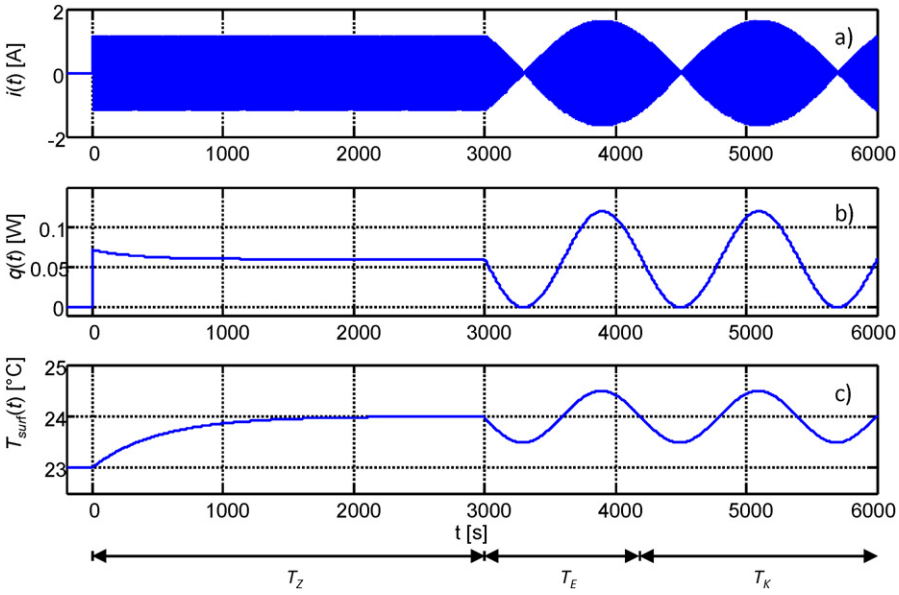

Fig. 3. Simulation of the cell temperature (a) excitation current $i(t)$, (b) heat flow $q(t)$ and (c) surface temperature of the cell $T_{surf}(t)$ as functions of time. T_Z: transient time, T_E: delay time (periods are excluded from evaluation of thermal impedance) and T_K: integration time (relevant for calculation of thermal impedance).

during measurement time, thus avoiding unwanted temperature oscillations initiated by the temperature controlling device.

The excitation signal was provided by a function generator 33250A (Agilent, USA), signal amplification was performed by an SI1287 potentiostat (Solartron, UK). Both devices were connected via GPIB (General Purpose Interface Bus) with a personal computer (PC) and were controlled by proprietary software. Voltage and current, measured by the potentiostat, were recorded by a mixed signal oscilloscope MSO6014A (Agilent, USA). Both quantities were used to calculate the electrochemical impedance and applied heat flow on a personal computer with proprietary software. Fig. 4 shows the experimental setup with the connection of the different devices.

Thermocouples of type K were used for temperature measurement. The surface temperature on the back and front center casing of the cell was measured by surface thermocouples SFT1 and SFT2. All temperatures were monitored by a 34970A Data Acquisition Unit (Agilent, USA).

5. Results and discussions

5.1. Time-domain method

The cell was set at a constant temperature of 23 °C, a SOC of 20% was adjusted and the cell voltage was allowed to settle under open circuit conditions. At the time $t_0 = 0$ a sinusoidal current with an amplitude of $I_A = 1.8$ A was applied for 2000s. Fig. 5a shows the surface temperature of the cell for eight separate measurements, as monitored by SFT1 and SFT2. The temperature increase was reproducible and the temperature difference between front center and back center of the cell was less than 0.1 K at the end of the experiment. The algorithm [14] requires very low noise in the signal. Therefore, the measured signal quality was further improved by averaging the eight sequenced measurements, as shown in Fig. 5b.

As mentioned before, the increasing cell temperature is associated with a decrease of the ohmic part of the cell resistance (Fig. 6).

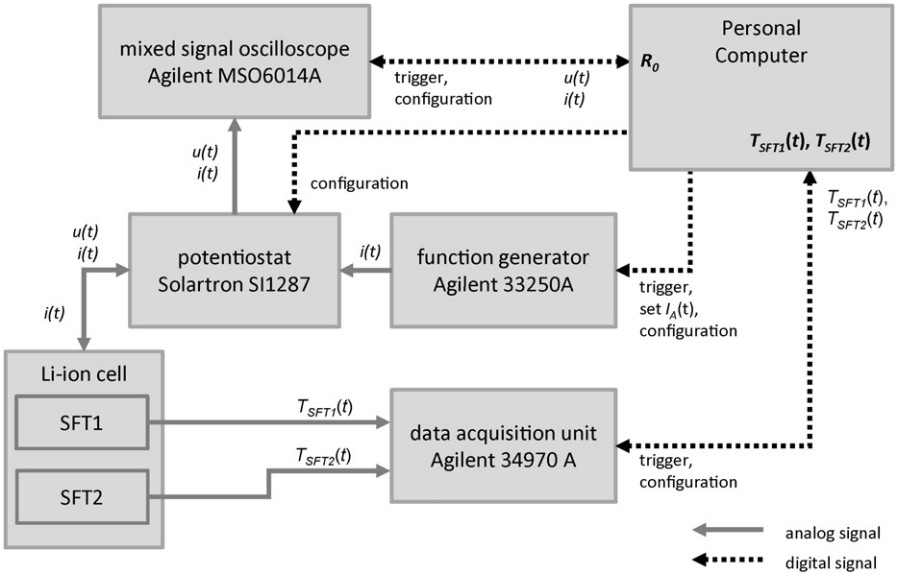

Fig. 4. Experimental setup for the electrothermal impedance spectroscopy (ETIS) on lithium-ion cells via time-domain and frequency-domain method.

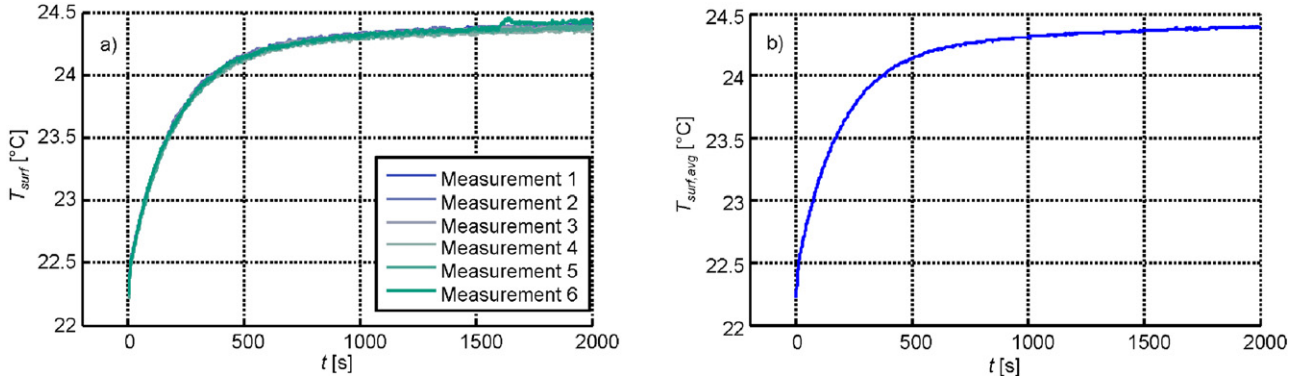

Fig. 5. (a) Surface temperature of the cell as functions of time, for six sequentially conducted identical measurements, showing good reproducibility of the measurements. (b) Averaged surface temperature of all six measurements as function of time, showing improved signal to noise ration to the single measurements. The stimulated flow generated is depicted in figure 6.

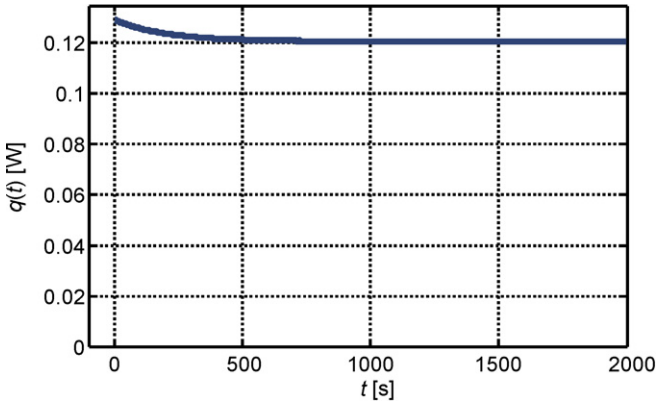

Fig. 6. Heat flow $q_{th}(t)$ versus time, stimulated by a sinusoidal current with constant amplitude $I_A = 1.8$ A.

Since the amplitude of the sinusoidal current is constant, the heat flow $q(t)$ generated by ohmic losses decreases. As shown in Fig. 7, this decrease in heat flow accounts to roughly 10%, which can be observed for all conducted experiments.

Now the thermal impedance is calculated with the algorithm described in [15]. The phase of the thermal impedance depicted in Fig. 8 shows instability for frequencies $f_q > 10$ mHz, thus indicating an upper limit of the time-domain method. The advantages of the time-domain method are (i) the short measurement time and (ii) the simple stimulation signal, which is easy to put into practice.

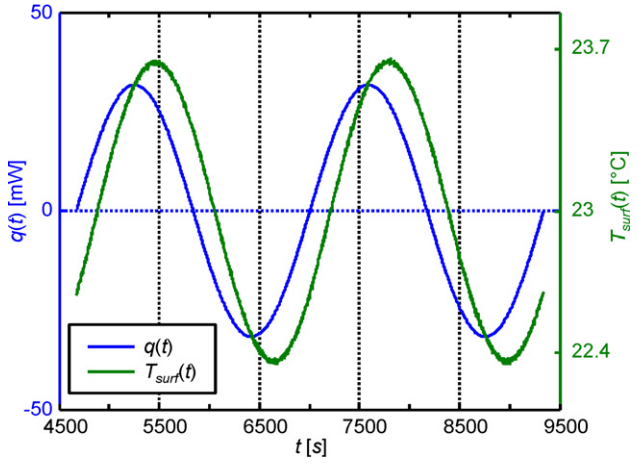

Fig. 7. Heat flow q and surface temperature T as functions of time during the modulation phase for the frequency $f_q = 423$ μHz.

5.2. Frequency-domain method

As for the measurements with the time-domain method, the cell was set at a constant temperature of 23 °C, a SOC of 20% was adjusted and the cell voltage was allowed to settle under open circuit conditions. Then at $t_0 = 0$ a sinusoidal current with a constant amplitude of $I_A = 0.9$ A was applied for a settling time of $T_Z = 3000$s (compare Fig. 3). Since the maximum current of the potentiostat at the frequency of the current oscillation $f_i = 17$ kHz is 1.8 A, a stationary heat flow at a constant amplitude of $I_A = 0.9$ A has to be established to allow for a maximum amplitude of the modulation of 0.9 A (compare Eq. (8)).

The experiment was conducted for 14 logarithmically spaced frequencies f_q in the range from 162 μHz to 89 mHz. Since the temperature signal has to be sampled in accordance with the Nyquist–Shannon sampling theorem [17], a sampling frequency f_s of

$$f_s > 2\max(f_q) \tag{11}$$

is required for a maximum frequency of $f_q = 89$ mHz. Since Eq. (11) is only correct for an infinite long observation of the signal, a higher sampling frequency has to be chosen in practice. Therefore sampling frequencies were chosen depending on the stimulated heat flow frequency f_q as shown in Table 1. A higher sampling rate results in an increased noise level of the temperature signal. To compensate for that, the number or periods for integration N_p was adapted to the sampling frequency. At lower frequencies noise suppression of the temperature measurement is very good. In this case smaller values for N_p are sufficient.

The relation of delay time T_E and integration time T_K was chosen as

$$\frac{T_E}{T_K} = \frac{2}{1} \tag{12}$$

Following Eq. (12), the number of periods for integration N_p was calculated as

$$N_p = \left\lfloor \frac{2}{3} N \right\rfloor \tag{13}$$

The duration of the complete measurement was one day. Fig. 7 shows the derived heat flow and the measured surface temperature for an excitation frequency of 423 μHz and maximum amplitude of the excitation current oscillation of 1.8 A. Both signals show a very high data quality and are perfect sinusoidal functions.

The measurement results obtained from the frequency-domain method are in good accordance with those obtained from the time-domain method (compare Fig. 8). The superiority of the frequency-domain method is clearly visible as the phase of the

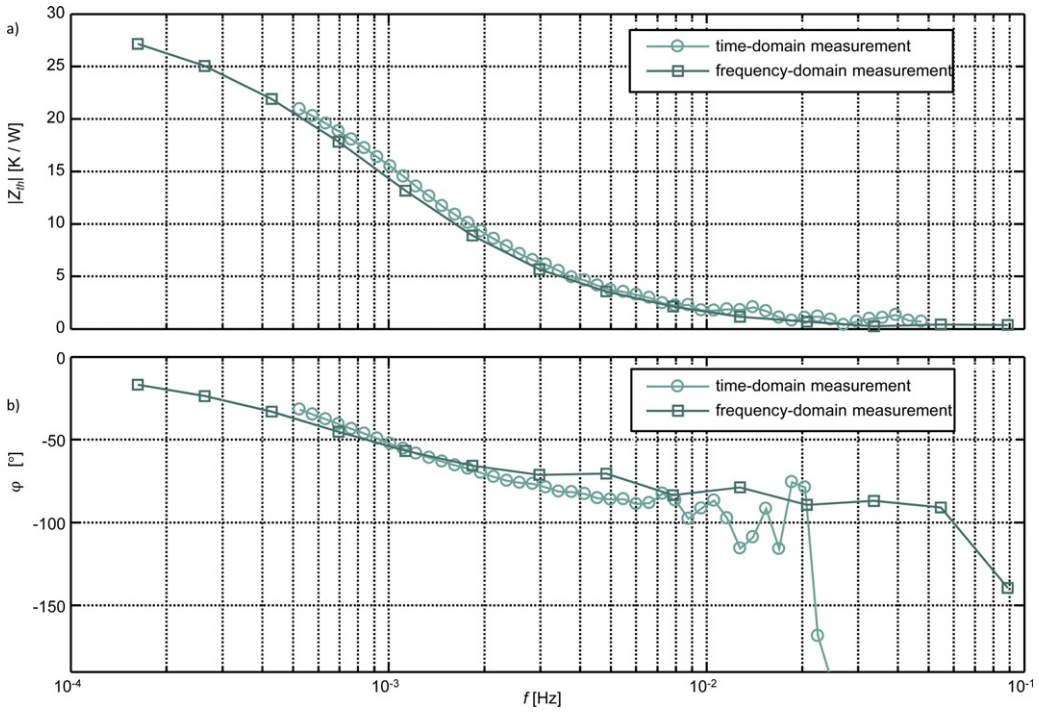

Fig. 8. (a) Magnitude of the thermal impedance Z_{th} obtained by time-domain and frequency-domain measurement over frequency, (b) phase φ of the thermal impedance Z_{th} obtained by time-domain and frequency-domain measurement over frequency.

frequency-domain measurement spectrum is even stable at frequencies $f_q > 10$ mHz, which allows to extend the frequency range by one decade. At the highest measured frequency of 89 mHz, the phase angle decreases below −90°. Since the magnitude approaches zero for high frequencies, the phase angle is hardly measurable. For this reason, the measured value at 89 mHz were excluded from interpretation.

Furthermore, we cannot completely exclude a drift in the surrounding temperature for frequencies $f_q < 1.62\text{E}{-4}$ Hz. The test setup has to be improved first to enable measurements at even lower frequencies with the frequency-domain method.

Nevertheless both methods are valid for the direct experimental determination of the thermal impedance of Li-ion cells, and can be applied independent from size, geometry, and design.

The time-domain method is faster as the frequency-domain method, but requires a complex mathematical transformation to calculate the thermal impedance. Using the frequency-domain method, the impedance can be easily read from the sinusoidal heat flow and temperature signal. Furthermore the noise suppression can be configured individually for each frequency f_q by adjusting the number of integration periods. For both methods no assumptions or models are necessary for the correct calculation of the generated heat flow. The obtained thermal impedance spectra can be used to (i) deduce a model structure, (ii) validate models and (iii) parameterize impedance models. Methods such as complex nonlinear least square (CNLS) fits, well-established from electrochemical modeling, can be applied for the interpretation of the obtained spectra.

As the position of the thermocouple is varied, different thermal impedances for different positions can be obtained. This is the basis for a spatially resolved thermal impedance model.

Recently Forgez et al. [9] published results on the thermal behavior of cylindrical cells. The cells were excited with symmetrical current impulses at a frequency of 2 Hz. This method also creates a heat flow to the cell without the need for external heat stimulation. Symmetrical current pulses give rise to a quasi-constant SOC condition. The heat flow was calculated as the difference between cell potential V and equilibrium U_{avg} potential [18]:

$$q = I(V - U_{avg}) \tag{14}$$

However, this formula is only valid for an electrical circuit model which only contains an ohmic resistance. As the internal resistance of a lithium-ion cell is a complex impedance expression, the power has to be divided in real power and reactive power. Since only the real power contributes to heat generation, Eq. (14) is an approximation.

Additionally, it should be considered that an excitation signal of 2 Hz may lead to changes in entropy and therefore to a change in temperature due to stimulation of the intercalation process [13].

Table 1
Sampling frequencies f_s (sampling rate for the temperature), total number of stimulated periods N and number of periods for integration N_p for different stimulated frequencies of heat flow f_q.

f_q [Hz]	1.62^{-4}	2.64^{-4}	4.28^{-4}	6.95^{-4}	1.13^{-3}	1.83^{-3}	2.98^{-3}
f_s [Hz]	0.25	0.5	0.5	0.5	1	1	1
N	3	3	4	4	5	5	5
N_p	2	2	2	2	3	3	3
f_q [Hz]	4.83^{-3}	7.85^{-3}	1.27^{-2}	2.07^{-2}	3.36^{-2}	5.46^{-2}	8.86^{-2}
f_s [Hz]	1	1	2	2	2	2	2
N	8	8	10	10	10	20	20
N_p	5	5	6	6	6	13	13

This process must then be included in a coupled electrochemical model.

Furthermore, this approach requires the opening of the cylindrical cell, as a thermocouple was placed in the center of the roll to measure the internal cell temperature. The equivalent circuit model was parameterized with the data gained from the internal thermocouple and the one placed on the surface. Obviously, this approach is not applicable for pouch-cells.

A thermal cell model without the need to parameterize an electrochemical one was shown first by Barsoukov et al. [12]. This approach uses a heating band wound around a cylindrical cell and a thermocouple placed on the cell surface. The heat flow step applied to the surface was calculated as the electrical power dissipation of the heating band. To obtain an expression in frequency domain, the time domain signals were fitted to a sum of exponential functions. However this method is restricted to stimulations with a step in heat flow and it is based on the assumption of a model. As the underlying model is deduced from the cylindrical geometry, the approach is restricted to cylindrical cells. Furthermore, the position of heat generation during the experiment (heat band outside the cell) does not coincide with heat generation during cell operation.

6. Conclusions

A new method, named electrothermal impedance spectroscopy (ETIS), was presented as a non-destructive procedure to measure the thermal impedance of lithium-ion cells directly. It uses an oscillating current (frequency 17 kHz) to create heat within the cell. The thermal impedance can be calculated from the change in surface temperature, and is the basis for a thermal cell model, describing the transient and stationary temperature behavior. The obtained thermal impedance spectra can be used to (i) deduce a model structure, (ii) validate models and (iii) parameterize impedance models. By fitting the thermal impedance to an equivalent circuit, easy implementable and fast models for onboard functions of EV or HEV can be developed. Assumptions on model structure are not necessary, which is advantageous compared to thermal modeling presented to far.

ETIS can be performed likewise in time-domain and in frequency-domain measurements. The time-domain method is faster, but the thermal impedance has to be calculated with the help of a complex mathematical transformation. The frequency-domain method obtains the thermal impedance directly by reading the sinusoidal heat flow and the corresponding temperature signal at the same time.

An application of ETIS to whole battery packs is also possible and should be investigated in the near future.

Acknowledgements

The German Federal Ministry of Education and Research (BMBF PTJ-03SF0343H) and the CFN (Project F2.1) are acknowledged for financial support.

References

[1] T.D. Hatchard, D.D. MacNeil, A. Basu, J.R. Dahn, J. Electrochem. Soc. 148 (2001) A755–A761.
[2] Y.F. Chen, J.W. Evans, Electrochim. Acta 39 (1994) 517–526.
[3] G.G. Botte, R.E. White, Z.M. Zhang, J. Power Sources 97–98 (2001) 570–575.
[4] B. Markovsky, A. Rodkin, Y.S. Cohen, O. Palchik, E. Levi, D. Aurbach, H.J. Kim, M. Schmidt, J. Power Sources 119 (2003) 504–510.
[5] J. Vetter, P. Novak, M.R. Wagner, C. Veit, K.C. Moller, J.O. Besenhard, M. Winter, M. Wohlfahrt-Mehrens, C. Vogler, A. Hammouche, J. Power Sources 147 (2005) 269–281.
[6] L. Song, J.W. Evans, J. Electrochem. Soc. 147 (2000) 2086–2095.
[7] P.M. Gomadam, R.E. White, J.W. Weidner, J. Electrochem. Soc. 150 (2003) A1339–A1345.
[8] M. Fleckenstein, O. Bohlen, M.A. Roscher, B. BΣker, J. Power Sources 196 (2011) 4769–4778.
[9] C. Forgez, D.V. Do, G. Friedrich, M. Morcrette, C. Delacourt, J. Power Sources 195 (2010) 2961–2968.
[10] M. Jakob, Heat Transfer, Wiley, New York [u.a.], 1919, Ref. type: Serial (Book, Monograph).
[11] Y. Hu, S. Yurkovich, Y. Guezennec, B.J. Yurkovich, J. Power Sources 196 (2011) 449–457.
[12] E. Barsoukov, J.H. Jang, H. Lee, J. Power Sources 109 (2002) 313–320.
[13] J.P. Schmidt, T. Chrobak, M. Ender, J. Illig, D. Klotz, E. Ivers-Tiffée, J. Power Sources 196 (2011) 5342–5348.
[14] D. Klotz, M. Schönleber, J.P. Schmidt, E. Ivers-Tiffée, Electrochim. Acta, submitted for publication.
[15] K. Takano, K. Nozaki, Y. Saito, A. Negishi, K. Kato, Y. Yamaguchi, J. Power Sources 90 (2000) 214–223.
[16] M.E. Orazem, B. Tribollet, Electrochemical Impedance Spectroscopy, John Wiley & Sons, Inc., Hoboken, NJ, 2008.
[17] C.E. Shannon, Proc. Inst. Radio Eng. 37 (1949) 10–21.
[18] K.E. Thomas, C. Bogatu, J. Newman, J. Electrochem. Soc. 148 (2001) A570–A575.